

A somatotopic map of vibrissa motion direction within a barrel column

Mark L Andermann¹ & Christopher I Moore²

Most mammals possess high-resolution visual perception, with primary visual cortices containing fine-scale, inter-related feature representations (for example, orientation and ocular dominance). Rats lack precise vision, but their vibrissa sensory system provides a precise tactile modality, including vibrissa-related ‘barrel’ columns in primary somatosensory cortex. Here, we examined the subcolumnar organization of direction preference and somatotopy using a new omni-directional, multi-vibrissa stimulator. We discovered a direction map that was systematically linked to somatotopy, such that neurons were tuned for motion toward their preferred surround vibrissa. This sub-barrel column direction map demonstrated an emergent refinement from layer IV to layer II/III. These data suggest that joint processing of multiple sensory features is a common property of high-resolution sensory systems.

A ‘map’ of the sensory periphery is a consistent and defining organizational principle of primary sensory cortices^{1,2}. In the primary visual cortex (V1) of most mammals, multiple systematic representations, reflecting distinct sensory features, have been reported. For example, ocular dominance and orientation columns are coextensive with a retinotopic map in V1 of the cat and monkey^{3–6}. The features of the visual scene represented in these maps suggest their importance for solving the behavioral problems faced by a given species. Further, their specific horizontal and laminar organization is believed to be important to the computations conducted in cortex^{7–9} and to provide insight into the mechanisms by which maps are established and maintained in development and in adulthood^{10,11}.

Rats and mice lack the visual capacity of most other mammals¹², and their primary visual cortices do not demonstrate systematic maps of features such as orientation^{6,13}. In contrast, the rodent’s facial vibrissae provide a high-resolution sensory system, capable of making precise discriminations. During active perception, rats ‘whisk’ multiple vibrissae against surfaces at a rate of ~8 Hz (ref. 14). This behavior suggests the rapid sensory integration of somatotopic, multi-vibrissa cues with feature information from single vibrissae^{15–17}. One potentially important cue is the direction of vibrissa motion, which will vary as a rat’s vibrissae contact distinct object shapes¹⁸.

In agreement with the putative utility of these features, vibrissa receptive fields in primary somatosensory cortex (SI) can be characterized by their somatotopic tuning—the distribution of vibrissae that drive neural activity—and their direction preference—the optimal angle of vibrissa deflection¹⁹ (Fig. 1a,b). Somatotopy is well known to exist in an organized anatomical map in SI, with a one-to-one association between vibrissae and layer IV barrels²⁰. Sub-barrel somatotopy also has been observed: lateral location within a barrel column

predicts the nearest-neighbor surround vibrissa that has the second strongest input (after the primary vibrissa)²¹.

There is currently no evidence that vibrissa direction preference is organized in a systematic anatomical map or has a consistent relation to somatotopy. Several plausible models exist for the possible relation between somatotopic tuning (and, in turn, anatomic position in a vibrissa column) and direction preference, with first-order predictions being that these features will be correlated or anticorrelated. According to the correlated hypothesis, direction preference at a given site is biased toward the nearest somatotopic neighbor, forming an outward radiating pattern within the vibrissa column (Fig. 1c, model 1). According to the anticorrelated hypothesis, direction preference is for motion away from the nearest somatotopic neighbor (Fig. 1c, model 2). Support for either model comes from a consideration of the integration of directional and somatotopic cues during active perception. When a vibrissa is deflected in a given direction, it moves into the spatial, somatotopic region represented by a specific neighboring vibrissa. Consistent synchrony of the neural activity evoked by these two inputs as they sample similar or identical regions of space could, under a Hebbian mechanism, lead to the binding of these features²². Conversely, if such correlated interactions evoked, instead, an offset in the precise timing of firing, then a depression of synaptic efficacy in driving their common targets might emerge²³. Further motivation for these models is provided by consideration of peripheral receptor organization^{24,25} and skin mechanics. A third hypothesis posits that direction tuning and somatotopy have no interdependence and that a random assortment of direction preferences exists across somatotopic space (Fig. 1c, model 3). In support of this model, previous studies of layer IV barrels have reported a disorganized array of direction preference clusters of neurons that has no consistent association with somatotopy²⁶.

¹Harvard Program in Biophysics, Medical School Campus, Building C-2 Room 122, 240 Longwood Avenue, Boston, Massachusetts 02115, USA. ²McGovern Institute for Brain Research and Department of Brain and Cognitive Sciences, 46-2171 Massachusetts Institute of Technology, Cambridge, Massachusetts 02139, USA. Correspondence should be addressed to C.I.M. (cim@mit.edu).

Received 3 November 2005; accepted 23 February 2006; published online 19 March 2006; doi:10.1038/nn1671

Here, we report the discovery of a direction preference map existing within a barrel column that parallels the correlated model prediction. Using a new vibrissa stimulator and multielectrode recordings, we observed that direction preference was predicted by anatomical position within the barrel column and by the somatotopic receptive field of the neuron. This map was more robust in the supragranular layers, suggesting that it is an emergent property of the cortical circuit.

RESULTS

Receptive field mapping

Using a nine-vibrissa stimulator centered on the D3 vibrissa, we made recordings at several depths and lateral locations with a four-tetrode array (Fig. 1a,b and Supplementary Fig. 1 online). Spatial and directional receptive fields were delineated by stimulating one of the nine vibrissae in one of eight directions every 125 ms in a random, counterbalanced order ($N = 192$ single units; $N = 225$ multi-unit sites; $N = 11$ rats and experiments; Methods). We conducted analyses only on sites within the D3 vibrissa barrel column. With this approach, the somatotopic position of the receptive field and its direction preference were measured in a rapid and spatially symmetric fashion across all recordings.

Direction map in anatomic coordinates

Inspection of the direction preference map for regular-spiking units (RSUs: putative excitatory cortical neurons²⁷) suggested that direction preference varies as a function of position within the barrel column, such that direction preference toward an adjacent vibrissa is represented by neurons located nearest the corresponding adjacent barrel column (Fig. 1d). To test the model predictions, we calculated the angle of a given recording position relative to the center of the barrel and compared this metric with the direction preference of the neuron (Fig. 1e, inset). An angular-angular correlation²⁸ revealed that these two metrics were significantly correlated ($r = 0.226$; $P < 0.001$, $N = 26$ penetrations (48 neurons), 4 experiments).

A second way to assess the agreement between the correlated model and the direction map is to calculate the absolute value of the difference between the angular vectors for position and direction. In the strongest form of the correlated model, these angles should be identical; under the anticorrelated model, a 180° difference is predicted; and under the 'random' hypothesis, a 90° mean difference is predicted (chance association). The mean difference in angle between direction preference and anatomical barrel position was significantly smaller than 90° ($P < 0.0001$; Fig. 2a). To control for any biases that may have been intrinsic

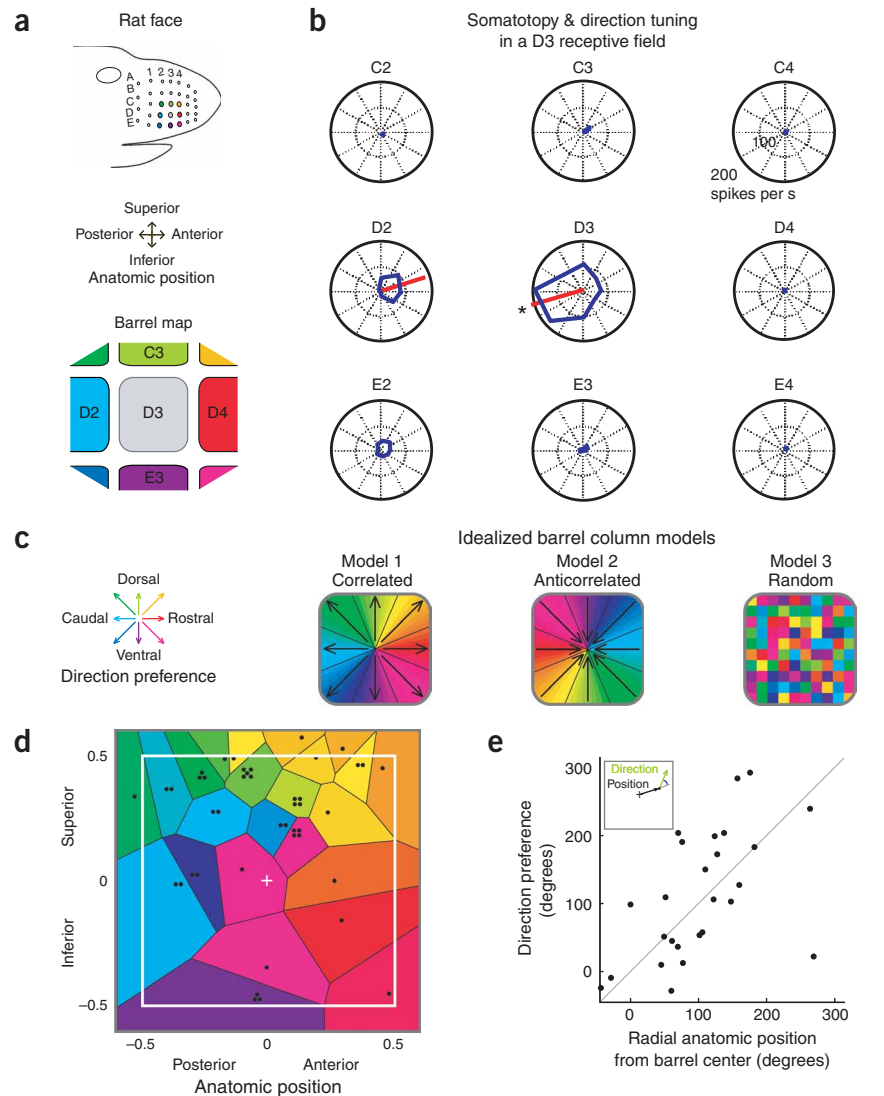


Figure 1 A sub-barrel direction map in anatomic coordinates. **(a)** Top: an idealized map of the rat face. Color indicates position of the stimulated vibrissae: the D3 and nearest neighbors. To ensure balanced sampling within and across experiments, data throughout are reported only for sites driven best by the D3 vibrissa and for D3 direction preferences. Bottom: a map of the position of the corresponding barrel columns in rat SI. **(b)** An SI multiunit receptive field with caudal-ventral D3 vibrissa directional responses (central blue tuning curve) and a posterior somatotopic bias toward the D2 vibrissa. Black asterisk, somatotopic center of mass (centroid of the mean firing rate evoked by each vibrissa). Red lines, direction preference (vector sum of responses across eight motion directions). **(c)** Three possible models of the relation of direction preference and somatotopy in a barrel column. In the correlated model, direction preference toward an adjacent vibrissa is represented by neurons located nearest the corresponding adjacent barrel, and the opposite relation holds in the anticorrelated model. In the random model, direction preference is unrelated to somatotopy or anatomic position in a vibrissa column. **(d)** The direction preference map made from single-unit recordings from layers II–IV shown relative to barrel coordinates (white box indicates barrel borders). When several single units were recorded within a penetration (indicated by multiple dots), direction preferences were averaged. For presentation, maps throughout are shown with a single smoothing of nearest-neighbor preferences, although all analyses were conducted on unsmoothed data. **(e)** A scatter plot showing the relation between direction preference and the radial anatomic position of the recording site (see inset). Data are shown without smoothing. The diagonal shows the unity line.

to this data set, we also shuffled data, so that recorded direction preferences were randomly assigned to recorded positions in the map. Shuffled data sets were not significantly different from chance ($P > 0.1$). Although the correlated model does not account for all

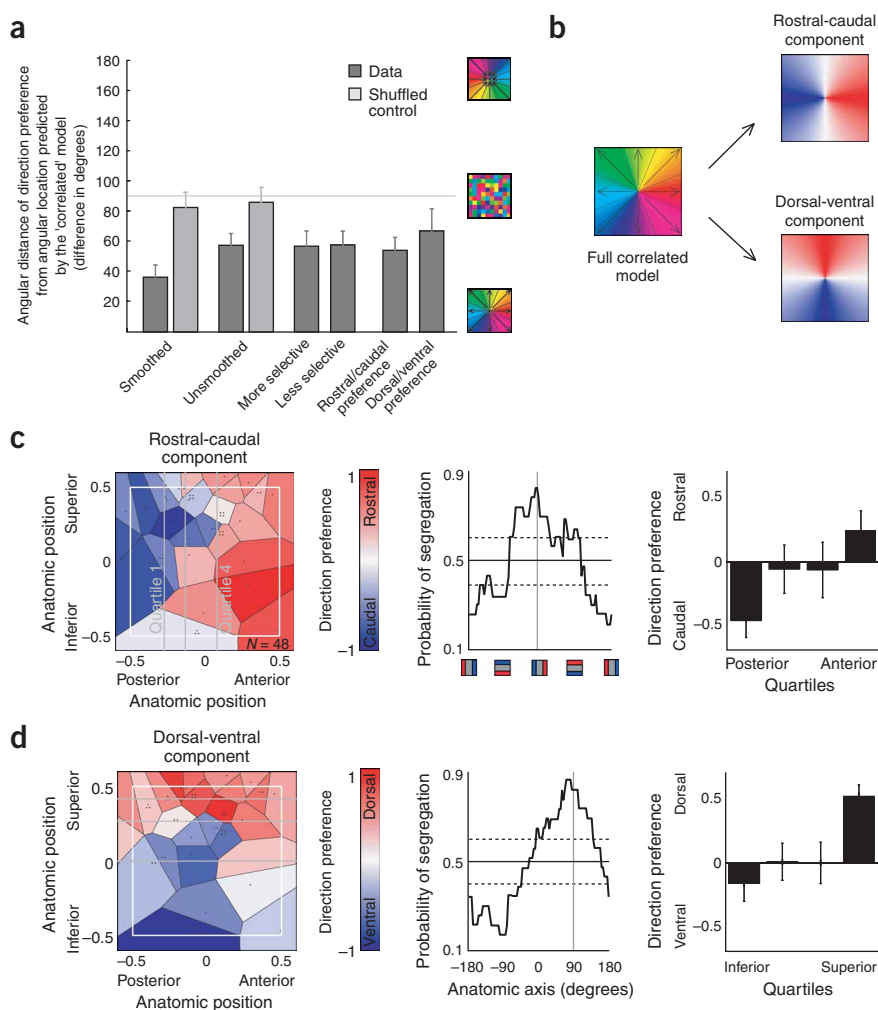


Figure 2 Analysis of the direction map for subpopulations of the data. **(a)** The difference between the spatial angle of a given site, relative to the center of a barrel column, and its direction preference. The data best match the prediction of the correlated hypothesis and are significantly different from the predictions of the anticorrelated (180° difference) and random (90° difference) models, when analyzed smoothed or unsmoothed. Light gray bars, identical analysis applied to shuffled data (smoothed and unsmoothed). This analysis was also conducted using subgroups of neurons showing higher or lower direction selectivity, or showing dorsal-ventral (DV) or rostral-caudal (RC) direction preference. Error bars represent s.e.m. throughout. **(b)** To further analyze whether the correlated direction map was expressed along both cardinal axes, direction preference at each recording position was decomposed into dorsal-ventral and rostral-caudal components. **(c,d)** Left: the rostral-caudal and dorsal-ventral component maps. Center: line plots showing the probability of segregation of cells preferring rostral-caudal or dorsal-ventral directions in outer quartiles (1 and 4) as a function of the angle of rotation of the axis of separation, such that 0° indicates the posterior-anterior axis (Results and Methods). Vertical gray bars, optimal segregation. Solid and dashed horizontal black lines, mean and s.d. of probabilities for shuffled data, respectively. As predicted by the correlated model, the dorsal-ventral map was fit optimally at an angle of -7.2° (0° predicted) and the rostral-caudal map at an angle of 82.8° (90° predicted). Right: data for the dorsal-ventral or rostral-caudal direction preference, averaged within each of the quartiles and taken at the optimal angle of segregation. The outer quartiles showed significantly different mean direction preferences.

angular variance, these findings support this hypothesis and significantly differ from the predictions of a random or anticorrelated map.

We next investigated whether the correlated direction map was exclusively dependent on subpopulations of neurons with distinct response characteristics, such as high direction selectivity. The RSUs recorded in this study demonstrated relatively sharp direction tuning, a value of 2.32 ± 0.14 (mean \pm s.e.m., $N = 48$; calculated as the response in the best direction divided by the mean response to all directions²⁹). This value is above or near the top of the range reported in previous studies of RSU direction selectivity in rat SI (ref. 29). We confirmed adherence to the correlated model for subpopulations of cells with direction tuning higher and lower than the median tuning observed (Fig. 2a; angular difference: $P < 0.003$ for both, $N = 15$ and 17 penetrations, respectively (24 and 24 neurons); angular-angular correlation: $r = 0.211$ and 0.289 , $P < 0.001$).

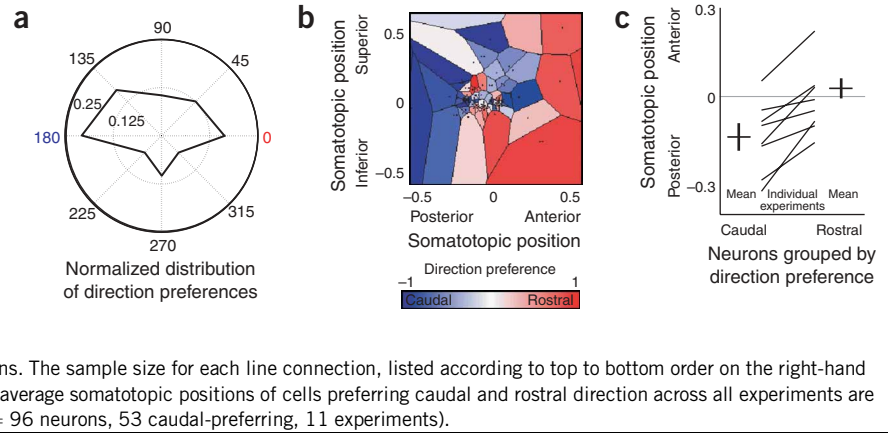
To test whether these systematic associations held for both cardinal direction preference axes (rostral-caudal and dorsal-ventral), we performed angular-angular correlations and angular difference calculations on neurons preferring rostral or caudal motion (RC), or dorsal or ventral motion (DV). Both groups revealed a significant angular-angular correlation (RC: $r = 0.34$, $P < 0.001$, $N = 19$ sites (28 neurons); DV: $r = 0.029$, $P < 0.05$, $N = 13$ sites (20 neurons)). The RC group showed a significant angular difference from shuffled data ($P = 0.0003$), and the DV showed a marginally significant effect ($P = 0.0658$; Fig. 2a).

We then generated direction preference maps for each axis, considering the rostral-caudal and dorsal-ventral components of direction preference separately across all RSUs (Fig. 2b–d; Methods). To analyze the angular agreement with the correlated model, we segmented the direction map into quartiles and calculated the optimal axis for separation of the first and fourth quartiles into caudal and rostral-prefering domains or ventral and dorsal-prefering domains. Under this analysis, the correlated model predicts a dorsal-ventral map with an axis orientation of 90° and a rostral-caudal map with an axis orientation of 0° (Fig. 2b). The dorsal-ventral map showed an axis orientation of 82.8° and the rostral-caudal map of -7.2° , and both maps showed a significant difference in the net direction preference of the outer quartiles (rostral-caudal map at 0° axis orientation: difference in rostral-caudal preference = 0.7 , $P = 0.001$; dorsal-ventral map at 90° axis orientation: 0.67 , $P = 0.0003$; N per quartile = 12). Further, knowledge of a cell's location within a quartile predicted its direction preference (the probability of rostral preference for the posterior quartile = $2/11$ (18%); $P(\text{rostral} | \text{anterior}) = 7/12$ (58%); $P(\text{dorsal} | \text{inferior}) = 3/11$ (27%); $P(\text{dorsal} | \text{superior}) = 11/12$ (92%); data not shown).

Rostral-caudal direction preference bias

Although we observed a correlated map for both axes, this finding does not mean that there was an equal distribution of DV and RC tuning preferences. Somatotopic receptive fields have a predominance of input

Figure 3 Rostral-caudal direction preference maps. **(a)** The distribution of single-unit direction preferences, calculated from the vector sum and binned across eight directions. A bias to rostral or caudal vibrissa motions was observed. **(b)** Direction preference data plotted relative to the somatotopic center of mass ($N = 96$ RSUs, 11 experiments). The somatotopic center of mass was determined by the weighted average response across all nine vibrissae (Methods). **(c)** In all experiments where both caudal and rostral direction preferences were observed, caudal-prefering neurons had somatotopic receptive fields that were more posterior ($N = 8$ of 8). Individual experiments are indicated by line connections. The sample size for each line connection, listed according to top to bottom order on the right-hand side, was 16, 15, 9, 8, 12, 16, 7 and 7 neurons. The average somatotopic positions of cells preferring caudal and rostral direction across all experiments are shown as solid horizontal bars in the outer panels ($N = 96$ neurons, 53 caudal-prefering, 11 experiments).



from vibrissae within a row^{30,31}. If direction preference and somatotopy are correlated, a similar anisotropy would be predicted for direction preference. We observed a rostral-caudal bias in direction preference, as RSUs tuned for rostral or caudal motion toward vibrissae in the same row were over twice as prevalent as those tuned for motion toward neighboring vibrissae dorsal or ventral to the D3 vibrissa (RC: $N = 18$ of 48 (38%); DV: $N = 8$ of 48 (17%); **Fig. 3a**).

This dominance of RC preferences represents a systematic anisotropy in the data and is in disagreement with the idealized correlated model (**Fig. 1**). Reflecting this bias, we conducted subsequent analyses using the rostral-caudal component of direction preference.

Direction map in somatotopic coordinates

The analyses conducted thus far support a relation between anatomic position and direction preference but do not explicitly compare somatotopy and direction preference. One of the primary motivations for the correlated model was the potential coregistration of these two features. We therefore assigned recordings to their position in somatotopic space, an analysis made possible by the balanced sampling of the entire nine-vibrissa receptive field for each recording. This

‘conceptual map’ provides a direct representation of the features under comparison. As predicted by the close correlation of anatomic position and somatotopic tuning along the anterior-posterior axis²¹ (**Supplementary Fig. 2** online), an RC gradient in RSU direction preference was evident in somatotopic coordinates (**Fig. 3b**). In all experiments where rostral and caudal direction preferences were recorded ($N = 8$),

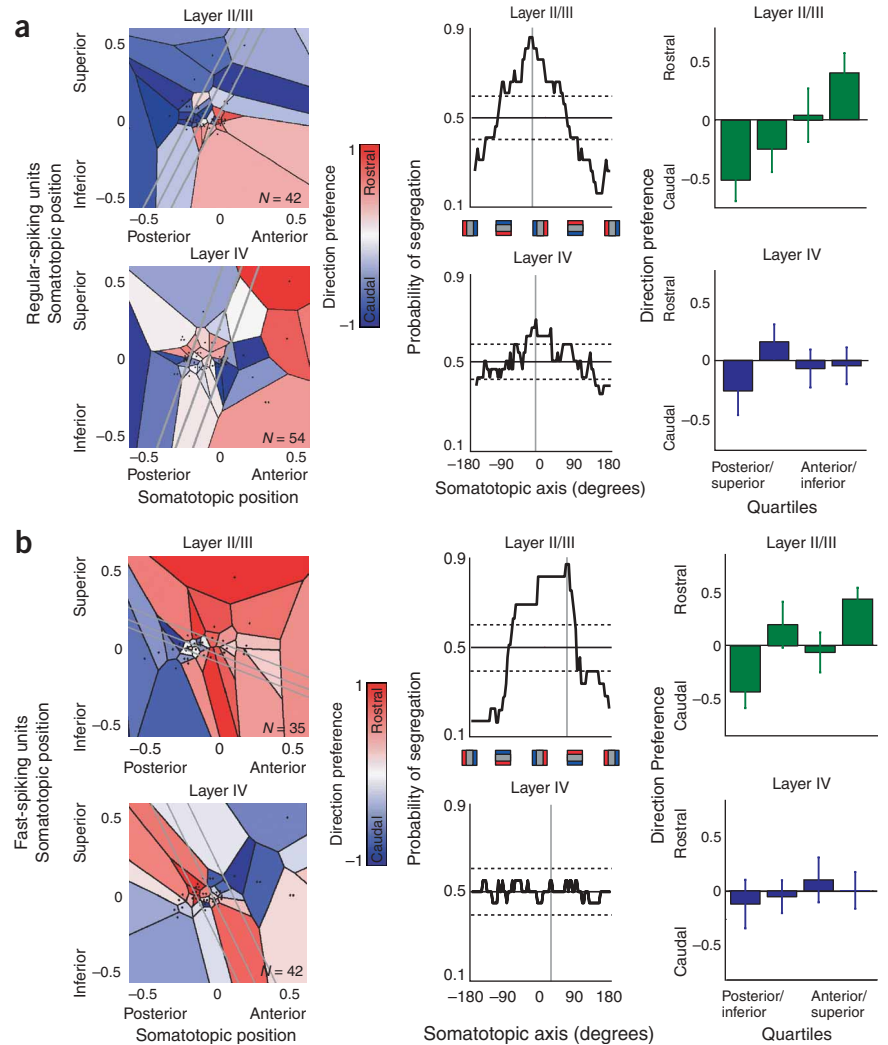


Figure 4 Direction preference maps in layers IV and II/III for regular- and fast-spiking units. **(a)** Left: the RSU direction preference maps for layers II/III ($N = 42$ neurons) and IV ($N = 52$). Gray lines divide recordings into quartiles along the axis of optimal separation. Center: the probability of segregation of direction preferences of the outer quartiles, as described in **Figure 2**. Right: the average rostral-caudal direction preference of sites within a given quartile, taken parallel to the optimal axis of segregation. **(b)** The FSU direction map (layer II/III, $N = 35$; layer IV, $N = 42$). As with the RSU map, the FSU map showed a significant difference in direction preferences between the first and fourth quartiles in layer II/III and no association between map quartile and direction preference was evident in layer IV.

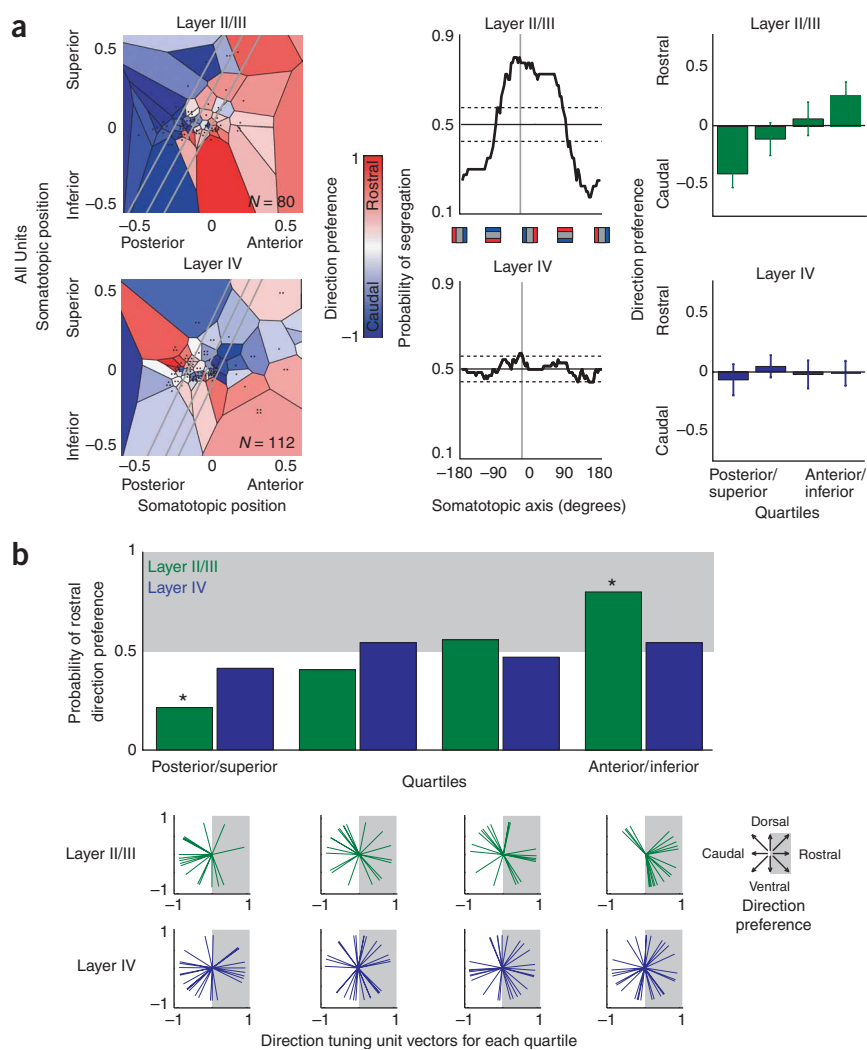


Figure 5 Direction preference maps in layers IV and II/III for all units. **(a)** Direction maps, probability of segregation and quartiles presented as in **Figures 2** and **4** for all single units combined. As in **Figure 4**, we observed significant differences in mean direction preference between outer quartiles in layer II/III but not in layer IV. **(b)** Top: the probability of rostral direction preference plotted for each quartile. Quartile boundaries are as in maps in **Figure 5a** (gray lines). Probabilities of rostral tuning were significantly less than chance in the posterior quartiles and significantly greater than chance in the anterior quartiles, in layer II/III but not in layer IV. Bottom: plots showing the direction preference of each neuron reported in this study, separated by layer and somatotopic quartile.

trend was observed in layer IV: under both analyses, the probability of finding the predicted rostral tuning in the anterior quartile was twice as great as that in the posterior quartile (nonrotated: 46% versus 23%; rotated: 54% versus 25%).

Analysis of other single-unit types yielded similar findings. The direction map, and the emergence of this map in supragranular layers, was also evident when fast-spiking units (FSUs: putative local inhibitory neurons^{27,32}) were considered alone (**Fig. 4b**; layer II/III: $N = 35$, difference in mean rostral-caudal preference = 0.66 for nonrotated ($P = 0.0016$), 0.79 for rotated 68° ($P = 0.0002$); layer IV: $N = 42$, -0.03 for nonrotated ($P = 0.45$), 0.12 for rotated by 25° ($P = 0.33$)). Further, the laminar segregation of the direction map was present when we pooled all neurons, including the small percentage that were not readily classified by unit type (**Fig. 5a**; layer II/III:

$N = 80$, 0.57 for nonrotated axis ($P = 0.0006$), 0.65 for rotated -29° ($P < 0.0001$); layer IV: $N = 112$, -0.02 for nonrotated ($P = 0.44$), 0.05 for rotated -25° ($P = 0.37$)). Analysis of multiunit activity (MUA) also indicated the presence of a map in layer II/III and further revealed a significant, albeit weaker, map in layer IV, in agreement with the trends observed in layer IV RSUs (**Supplementary Fig. 3** online).

Organization of the direction map within laminae

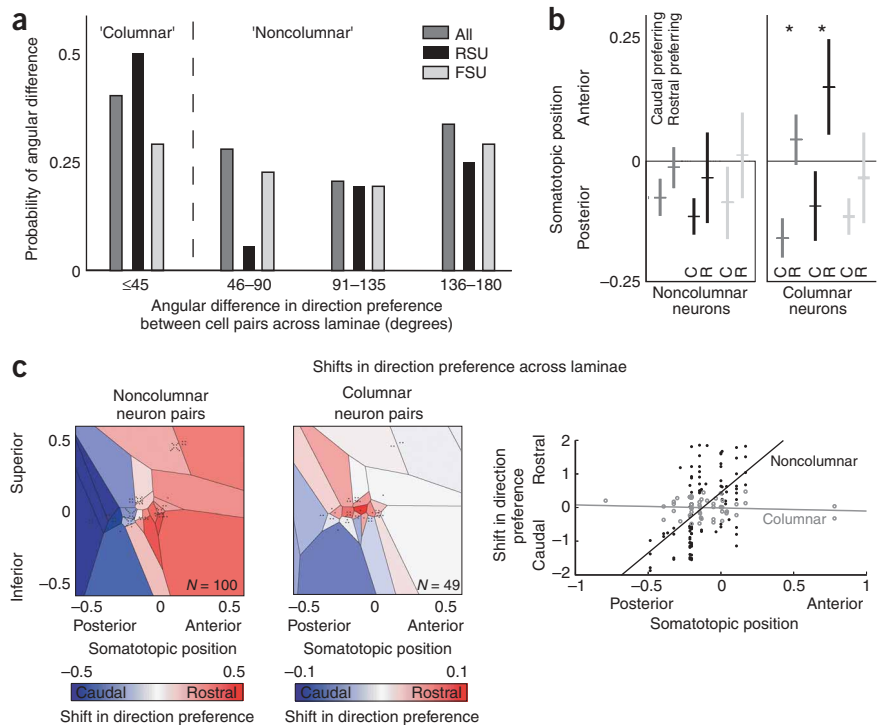
To assess the variance in direction preference as a function of somatotopy across all single units, we plotted individual direction preferences and the probabilities of rostral direction preference for each quartile of the maps (**Fig. 5b**). The incidence of caudal or rostral preference was significantly different from chance for the outer map quartiles in layer II/III (posterior quartile: probability = $4/19$ or 21%; anterior quartile: $15/19$ or 79%; $P < 0.02$ for both, sign test) but not in layer IV (posterior quartile: $11/27$ or 41%; anterior quartile: $15/28$ or 54%; $P > 0.4$ for both, sign test). Further, layer II/III showed a systematic increase in the probability of rostral tuning across quartiles, whereas layer IV did not (**Fig. 5b**).

These analyses show that an orderly direction map exists when analyzed in anatomic or somatotopic coordinates. We next asked whether this map is uniform at different cortical depths. Plots of RSUs recorded in layers II/III and IV suggested that the map is less organized in layer IV than in the supragranular layers (**Fig. 4**). Inspection of these maps also indicated that the principal axis of caudal to rostral preference may be tilted in somatotopic coordinates. Division of the layer II/III map along an axis rotated -27° from that of the idealized model yielded an optimal segmentation of the data. Analysis of nonrotated and rotated maps revealed a significant difference in direction preferences between quartiles in layer II/III ($N = 42$; difference in rostral-caudal preference = 0.79 for nonrotated ($P = 0.004$), 0.88 for rotated ($P < 0.0001$)). In neither case were layer IV RSU maps significant ($N = 54$; 0.18 for nonrotated ($P = 0.23$), 0.20 for rotated -20° ($P = 0.21$)). That said, a

Direction columns and the cross-laminar map transformation
To assess the columnar organization of the direction map and to examine its emergent reorganization across layers, we calculated the angular difference in direction preference for neurons recorded in

Figure 6 Consistency in direction preference across laminae predicts the correlation of direction tuning and somatopy. (a) To assess the columnar organization of direction tuning, the similarity in angular preference across depth was plotted for neuron pairs recorded within a single penetration between layer II/III and layer IV. The RSUs showed a bias toward agreement in direction tuning across layers ($\leq 45^\circ$ difference in tuning), indicating the existence of direction columns. Comparisons conducted across all neurons also showed a significant bias, but FSUs showed a flat distribution (details in text).

(b) Same analysis as shown in **Figure 3c**, applied to subpopulations of the data. For RSUs that showed agreement in direction tuning (a columnar arrangement), the rostral-caudal direction preference of a neuron predicted its somatopy. For noncolumnar pairs ($> 45^\circ$ difference in angular tuning), direction preference did not consistently predict somatopy. These findings were replicated when data were considered across all neurons, but were not observed in FSUs. (c) Left and middle: somatopy maps of the rostral-caudal shifts in direction preference across layers for all noncolumnar and columnar pairs of cells. Map coordinates indicate layer II/III somatopy. Note difference in color scale. Right: a scatter plot showing the relation between layer II/III somatopy and direction and magnitude of shift in preference. All pairs and linear regression fits were plotted for columnar (black closed circles) and noncolumnar (gray open circles) pairs (details in text). As indicated by both the map and scatter plot, the primary transformation of the map between layers is an increased rostral tuning for more anterior sites and increased caudal tuning for more posterior sites.



different laminae (layer II/III versus layer IV) within the same vertical penetration (**Fig. 6a**). Among pairs of RSUs, 18 of 36 pairs (50%) demonstrated similar direction preference ('columnar' pairs, $\leq 45^\circ$ difference between direction preferences; 'noncolumnar', $> 45^\circ$ difference). In contrast, pairs of FSUs did not show this bias, exhibiting a probability of agreement (9 of 31, 29%) approaching that expected by chance (25%). All neurons combined showed an intermediate distribution between the cell types (scatter plots of each neuron type in **Supplementary Fig. 4** online). The increased probability of similarity in tuning across layers among RSUs cannot be explained by distance between recording positions, as the distances between columnar-tuned RSU pairs and noncolumnar-tuned RSU pairs within a penetration were nearly identical ($N = 18$ for both; columnar: $347 \pm 25 \mu\text{m}$; noncolumnar: $356 \pm 21 \mu\text{m}$; $P = 0.4$). These findings suggest that vibrissa direction columns span laminae and are reflected in the activity of putative excitatory neurons.

The emergence of the layer II/III map is consistent with a model in which layer IV sites that show a correlation between somatopy and direction preference preserve their identity across laminae, forming columns of similarly tuned RSUs. To test this prediction, we analyzed cells that showed columnar direction agreement and asked whether their direction tuning predicted their somatopy tuning (**Fig. 6b**). For RSUs that agreed in their direction preference across layers (columnar), rostral-preferring neurons demonstrated significantly more anterior somatopy tuning than caudal-preferring neurons ($P = 0.03$, $N_{\text{caudal}} = 12$, $N_{\text{rostral}} = 15$). In contrast, for RSUs that did not show cross-laminar agreement (noncolumnar), direction preference did not consistently predict somatopy ($P = 0.28$, $N_{\text{caudal}} = 14$, $N_{\text{rostral}} = 10$). Consistent with the lack of interlaminar direction clustering among FSUs, neither category of FSU pairs demonstrated a significant link between direction preference and somatopy (columnar pairs:

$P = 0.21$, $N_{\text{caudal}} = 11$, $N_{\text{rostral}} = 13$; noncolumnar pairs: $P = 0.33$, $N_{\text{caudal}} = 4$, $N_{\text{rostral}} = 13$).

A corollary prediction of this model is that positions in the map that do not show columnar agreement instead demonstrate a net shift in tuning that supports the emergence of the map. Specifically, shifts in rostral tuning from layer IV to layer II/III should occur in the anterior portion of the somatopy map for noncolumnar sites, and shifts in caudal tuning should occur in the posterior portion. Maps of the directional shifts in tuning across layers revealed this effect for noncolumnar pairs but not for columnar pairs (**Fig. 6c** left and middle, and **Supplementary Fig. 5** online). Further, we observed a significant linear correlation across all cell pairs between directional shifts and layer II/III somatopy for noncolumnar sites ($r = 0.56$, $P < 0.0001$, $N = 100$; **Fig. 6c** right), but not for columnar sites ($r = -0.08$, $P = 0.28$, $N = 49$). This dissociation was also observed for RSUs and FSUs analyzed in isolation (**Supplementary Fig. 5**). This analysis confirmed that the predicted pattern of cross-laminar shifts largely arose from the non-columnar sites.

These findings suggest that a weakly correlated RSU map exists in layer IV and that the sites that support this map preserve their direction tuning, forming cross-layer columns with layer II/III. The positions in which directional and somatopy tuning are not correlated do not preserve their direction preference across layers and do not form columns. Instead, they demonstrate a systematic shift between layers, with anterior somatopy positions developing more rostral direction tuning and posterior positions developing more caudal direction tuning (**Supplementary Fig. 6** online).

DISCUSSION

The data presented here provide strong evidence for a systematic map of direction preference organized within a vibrissa column and for the

interdependence of somatotopic and directional representations. This direction map was biased toward rostral and caudal preferences and was more robust in layer II/III than in layer IV. These findings were supported by analyses across and within single experiments, when data were examined in anatomic or somatotopic coordinates, and were robust in single- and multiunit recordings.

When this sub-barrel direction map is considered in the context of the recently discovered resonance frequency columns³³, which span an arc of barrels, and the somatotopic barrel columns, these findings suggest that frequency, somatotopy and direction are systematically represented at distinct spatial scales in SI. These findings are in contrast to the absence of orientation or direction columns in rat primary visual cortex^{6,13}. This difference may reflect the relative importance of these sensory modalities to the behaving animal. Under this hypothesis, the high-acuity vibrissa sensory system requires computationally and metabolically optimized representations at fine resolution within SI (refs. 34,35), a selective pressure that does not apply in the rodent visual cortex. This organization may reflect the need to accurately represent multiple features in a single cortical area.

Whereas visual cortices of other mammals possess precise feature maps, these findings show that the barrel cortex is also distinct in that its vibrissa direction map correlates with the fine-scale representation of the sensory sheet. This corepresentation of features may enable more efficient sensory processing by placing two features that are correlated during active sensory perception in the same synaptic circuit. This proximity may facilitate the rapid and local amplification or suppression, depending on context, of statistical regularities during multi-vibrissa contact. Further, from a pragmatic viewpoint, because SI maps of somatotopy and direction can be localized relative to anatomic markers (barrels), they provide a unique opportunity for the examination of fine-scale cortical structure and function in a rodent model system.

As with many potential features encoded by the vibrissa sensory system, no study has conclusively determined that a rodent can use the direction of vibrissa motion as a sensory cue. Thus far, studies using stimuli that deflect vibrissae in multiple directions are confounded by alternate information (for example, multi-vibrissa interactions) that could account for the demonstrated acuity^{18,36}. Whereas definitive experiments have not been attempted, several lines of evidence support the assumption that rats can encode vibrissa directional information: these include the findings of the aforementioned behavioral studies, the high directional specificity of trigeminal neuron responses³⁷, the dynamic regulation of the selectivity of direction tuning in SI (refs. 29,38) and the demonstration of the systematically organized map reported here. The capability of the vibrissa sensory system is also suggested by the competence of single-vibrissa robotic systems, which demonstrate high-acuity shape discrimination even when using a single two-dimensional motion sensor (D.E. Kim & R. Moeller. *Proc. Int. Symp. Adaptive Motion in Animals and Machines*, 2005).

In this study, we intensively sampled the D3 vibrissa column, to facilitate the comparison of data across experiments. A key question is whether other vibrissa columns show different spatial organization. Variation in the properties of the vibrissae^{39–41}, and their potentially distinct role in encoding different kinds of information⁴², could lead to the development of a distinct sub-barrel column organization. The specialization of barrel columns relative to vibrissa identity is supported by variations in the patterns of cytochrome oxidase density within barrels across SI (ref. 43).

Several mechanisms may contribute to the emergence and maintenance of the observed direction map. Peripheral factors, such as the circular arrangement of receptors within the follicle²⁴ or cross-vibrissa interactions through the skin¹⁹, could help establish the cortical map. In

support of a subcortical contribution, direction preference is ordered in a thalamic barreloid⁴⁴. However, this barreloid representation is orthogonal to thalamic somatotopy, in contrast to the cortical association of these features, suggesting thalamo-cortical realignment. Further, the differences observed between layers IV and II/III suggest that cortical mechanisms transform map organization, consistent with data showing a cortical role in generating vibrissa direction preference^{26,32,45}.

The current findings provide specific support for the hypothesis that when vibrissae are deflected toward each other, they occupy common sensory space and generate synchronous firing in regions where their spatial receptive fields overlap. In turn, Hebbian correlation mechanisms could 'wire' regions of somatotopic overlap to predictive direction tuning. Our findings suggest that this association of features occurs, in part, through the enhanced or maintained synaptic efficacy of ascending columnar projections of those layer IV neurons whose directional tuning and somatotopic tuning are correlated. The preservation of feedforward inputs from layer IV to layer II/III could depend on the relative timing of lateral horizontal inputs from different surround columns that convey distinct somatotopic information⁴⁶. The plasticity of layer II/III in barrel cortex^{47–50} and the refinement of the direction map in layer II/III suggest a cortical locus for the integration of directional cues across multiple vibrissae.

METHODS

Surgery. Experiments were performed in compliance with protocols approved by the Massachusetts Institute of Technology. Male Sprague-Dawley rats ($N = 11$; mean weight \pm s.d.: 392 ± 35 g) were group housed ($N = 3–6$ rats) for ≥ 3 weeks in our standard caging, which includes multilevel surfaces, rodent tubes and a running wheel. Rats were anaesthetized with isoflurane (0.75–1.125% in 30% N_2O and 70% O_2), adjusted to maintain weak hindpaw withdrawal, constant heart rate and femoral blood pressure. After tracheotomy, rats were ventilated and placed on a floating table in a modified stereotax (Kopf), allowing free access to posterior vibrissae. A servo-controlled heating blanket maintained body temperature ($37^\circ C$). The left SI was exposed, and a retaining well was filled with warm saline. Rats were killed with an overdose of sodium pentobarbital and, in a subset, perfused in 4% paraformaldehyde.

Stimulation. The D3 vibrissa and eight adjacent vibrissae were stimulated by the motion of a multidirectional piezoelectric with attachments (**Supplementary Fig. 1**). Each stimulator was individually aligned to the resting axis of its vibrissa. A capillary tube was used for extension and a pulled glass electrode tip was inserted into the open end of the capillary (funnel pointing toward the piezoelectric). A trimmed vibrissa tip (length = ~ 7 mm) was secured in the point of the glass funnel, allowing directional motion of the vibrissa without additional transients or asymmetric torques⁴⁴. Voltage commands (MATLAB DAQ) were generated using I/O boards (NI), amplified (Sensor Technologies), and sent to piezoelectrics (Noliac). All stimulus waveforms consisted of merged half-sinusoids with fast rise (7 ms) and slow fall (50 ms), minimizing 'off' responses. Infrared sensors confirmed smooth motion profiles and the absence of resonant stimulator oscillations, and motion amplitudes were calibrated to $169 \pm 7 \mu m$ (mean \pm s.d.) across all directions and stimulators using a CCD camera (Nikon). To efficiently assess receptive fields, individual vibrissae were deflected every 125 ms. A run consisted of 73 stimulus types (8 directions \times 9 vibrissae + blank trials), presented 22 times in random order, with 3–9 runs per site. For most recordings, ramp-and-hold stimuli²⁶ were also presented (0.5 Hz presentation rate): these responses demonstrated similar direction preference and map properties (data not shown).

Electrophysiology. Single- and multiunit recordings (SU and MUA) were obtained using sharp-tipped multitetrode printed silicon probes (Michigan Probes/NeuroNexus; 2 shanks with 2 tetrodes each, 1–2 $M\Omega$ impedance, 150 μm spacing; see schematic in **Supplementary Fig. 1**). Recordings were sampled at 33.5 kHz (Neuralynx).

Tetrodes were presented normal to the cortical surface. Receptive field mapping was initiated in layer II/III (tetrode depths: 400 μm and 550 μm)

beginning > 10 min after entry. Tetrodes were then advanced 300 μm to layer IV (depths: 700 μm and 850 μm). In seven rats, several stimulation paradigms were presented, recordings at each depth lasted ≥ 1 h, and fewer positions were recorded in each experiment. In four rats, maps were assessed using a greater number of penetrations targeted to efficient mapping of somatotopy and direction preference. In these experiments, >90% of D3 vibrissa column penetrations were reconstructed after tangential sectioning of the cortex (80- μm slices) and Nissl and cytochrome oxidase staining. For coregistration across rats, we identified the anterior, posterior, superior and inferior borders of the D3 barrel (**Supplementary Fig. 1**) and skewed the y -axis ($\leq 20^\circ$) such that horizontal and vertical axes were orthogonal. The coordinates of the penetration locations were normalized such that values of -0.5 and 0.5 indicated posterior-anterior and inferior-superior barrel borders.

Analysis. RSUs and FSUs were clustered and sorted based on the ratio of peak-to-trough amplitude and the duration of the putative after-hyperpolarization^{27,33}. Spike waveforms exceeding 5 s.d. above background were included in MUA. A 0.5-ms minimum interspike interval between spikes on different tetrode contacts prevented repeated sampling of the same unit. Single-tetrode MUA—combining spike counts across the four contacts—was used in all MUA-based analyses.

Spike counts were averaged 5–15 ms after stimulus onset, capturing the ‘on’ response. Data were included if the mean response across all directions of D3 stimulation exceeded the mean response to any other vibrissa (that is, D3 was ‘primary’) and if significant evoked responses were present for at least one D3 motion direction (t -test, pre- versus poststimulus activity, SU: $P < 0.05$, MUA: $P < 0.01$).

To quantify ‘somatotopy’, we calculated the center of mass of the MUA response at a given site to the motion of nine vibrissae. In the following definitions, ‘arc’ refers to a dorsal-ventral oriented line of vibrissae within the grid on the rat face:

Horizontal somatotopic component = (summed anterior arc responses – summed posterior arc responses)/sum of all stimulated vibrissae.

Vertical somatotopic component = (summed superior row responses – summed inferior row responses)/sum of all stimulated vibrissae.

The range of both the horizontal and the vertical somatotopic components was -1 to 1 .

To quantify direction preference in the rostral-caudal axis, we calculated direction preference as follows:

Direction preference = ($|$ Angular distance of preferred direction from caudal $| - 90^\circ$)/ 90° . Range: -1 to 1 .

Shift in direction preference between layers = direction preference of layer II/III – direction preference of layer IV. Range: -2 to 2 .

For the analyses of rostral-caudal direction preference, cells were labeled as having caudal or rostral preference if their direction preference value was below or above zero, respectively. For anatomical analyses (for example, **Fig. 1e**), neurons at the same location (that is, on the same shank in the same layer) were averaged for map construction. For the analyses in **Figure 2a**, we used the mean direction preference vector across all relevant neurons (for example, dorsal- and ventral-tuned) recorded in a given penetration. For presentation, we generated tessellation plots using the Voronoi function (MATLAB); these were smoothed once (average of adjacent neighbor sites). For the quartile analyses in **Figures 2c, 4, 5a** and **Supplementary Figure 3**, we ordered somatotopic coordinates by their position along a given axis (0° = posterior-anterior = row axis). The probability of segregation was defined as follows: (number of caudal sites in quartile 1 + number of rostral sites in quartile 4)/(total number of sites in 1 and 4).

The axis angle was varied in steps of 3.6° from -180° to 180° , and the optimal angle was chosen to maximize the probability of segregation.

Unless otherwise stated, statistical tests were unpaired t -tests.

Note: Supplementary information is available on the Nature Neuroscience website.

ACKNOWLEDGMENTS

We thank J. Ritt, A. Nelson, M. Sur, C. Reid, R. Desimone and R. Born for feedback, and K. Kempadoo and A. Ramanathan for histology. We thank the US National Institutes of Health, the National Science Foundation, the McGovern Institute for Brain Research (C.I.M.) and the Howard Hughes Medical Institute (M.L.A.) for supporting this work.

COMPETING INTERESTS STATEMENT

The authors declare that they have no competing financial interests.

Published online at <http://www.nature.com/natureneuroscience>

Reprints and permissions information is available online at <http://npg.nature.com/reprintsandpermissions/>

- Head, H. *Studies in Neurology* (Oxford Univ. Press, London, 1920).
- Merzenich, M.M. & Kaas, J.H. Principles of organization of sensory-perceptual systems in mammals. *Progress in Psychobiology and Physiological Psychology* Vol. 9, 1–42 (Academic Press, San Diego, 1980).
- Hubel, D.H., Wiesel, T.N. & LeVay, S. Functional architecture of area 17 in normal and monocularly deprived macaque monkeys. *Cold Spring Harb. Symp. Quant. Biol.* **40**, 581–589 (1976).
- Hubener, M., Shoham, D., Grinvald, A. & Bonhoeffer, T. Spatial relationships among three columnar systems in cat area 17. *J. Neurosci.* **17**, 9270–9284 (1997).
- Blasdel, G.G. Orientation selectivity, preference, and continuity in monkey striate cortex. *J. Neurosci.* **12**, 3139–3161 (1992).
- Ohki, K., Chung, S., Ch'ng, Y.H., Kara, P. & Reid, R.C. Functional imaging with cellular resolution reveals precise micro-architecture in visual cortex. *Nature* **433**, 597–603 (2005).
- Yu, H., Farley, B.J., Jin, D.Z. & Sur, M. The coordinated mapping of visual space and response features in visual cortex. *Neuron* **47**, 267–280 (2005).
- Bosking, W.H., Zhang, Y., Schofield, B. & Fitzpatrick, D. Orientation selectivity and the arrangement of horizontal connections in tree shrew striate cortex. *J. Neurosci.* **17**, 2112–2127 (1997).
- Carreira-Perpinan, M.A. & Goodhill, G.J. Influence of lateral connections on the structure of cortical maps. *J. Neurophysiol.* **92**, 2947–2959 (2004).
- Ruthazer, E.S. & Stryker, M.P. The role of activity in the development of long-range horizontal connections in area 17 of the ferret. *J. Neurosci.* **16**, 7253–7269 (1996).
- Godecke, I., Kim, D.S., Bonhoeffer, T. & Singer, W. Development of orientation preference maps in area 18 of kitten visual cortex. *Eur. J. Neurosci.* **9**, 1754–1762 (1997).
- Prusky, G.T., West, P.W. & Douglas, R.M. Behavioral assessment of visual acuity in mice and rats. *Vision Res.* **40**, 2201–2209 (2000).
- Girman, S.V., Sauve, Y. & Lund, R.D. Receptive field properties of single neurons in rat primary visual cortex. *J. Neurophysiol.* **82**, 301–311 (1999).
- Carvell, G.E. & Simons, D.J. Biometric analyses of vibrissal tactile discrimination in the rat. *J. Neurosci.* **10**, 2638–2648 (1990).
- Ahissar, E. & Arieli, A. Figuring space by time. *Neuron* **32**, 185–201 (2001).
- Sachdev, R.N., Sellien, H. & Ebner, F. Temporal organization of multi-whisker contact in rats. *Somatosens. Mot. Res.* **18**, 91–100 (2001).
- Ghazanfar, A.A. & Nicolelis, M.A. Nonlinear processing of tactile information in the thalamocortical loop. *J. Neurophysiol.* **78**, 506–510 (1997).
- Pollay, D.B., Rickert, J.L. & Frostig, R.D. Whisker-based discrimination of object orientation determined with a rapid training paradigm. *Neurobiol. Learn. Mem.* **83**, 134–142 (2005).
- Simons, D.J. Temporal and spatial integration in the rat SI vibrissa cortex. *J. Neurophysiol.* **54**, 615–635 (1985).
- Woolsey, T.A. & Van der Loos, H. The structural organization of layer IV in the somatosensory region (SI) of mouse cerebral cortex. The description of a cortical field composed of discrete cytoarchitectonic units. *Brain Res.* **17**, 205–242 (1970).
- Armstrong-James, M., Fox, K. & Das-Gupta, A. Flow of excitation within rat barrel cortex on striking a single vibrissa. *J. Neurophysiol.* **68**, 1345–1358 (1992).
- Abbott, L.F. & Nelson, S.B. Synaptic plasticity: taming the beast. *Nat. Neurosci.* **3**, 1178–1183 (2000).
- Allen, C.B., Celikel, T. & Feldman, D.E. Long-term depression induced by sensory deprivation during cortical map plasticity *in vivo*. *Nat. Neurosci.* **6**, 291–299 (2003).
- Waite, P.M. & Jacquin, M.F. Dual innervation of the rat vibrissa: responses of trigeminal ganglion cells projecting through deep or superficial nerves. *J. Comp. Neurol.* **322**, 233–245 (1992).
- Wineski, L.E. Facial morphology and vibrissal movement in the golden hamster. *J. Morphol.* **183**, 199–217 (1985).
- Bruno, R.M., Khatri, V., Land, P.W. & Simons, D.J. Thalamocortical angular tuning domains within individual barrels of rat somatosensory cortex. *J. Neurosci.* **23**, 9565–9574 (2003).
- Bruno, R.M. & Simons, D.J. Feedforward mechanisms of excitatory and inhibitory cortical receptive fields. *J. Neurosci.* **22**, 10966–10975 (2002).
- Zar, J.H. *Biostatistical Analysis* (Prentice-Hall, Upper Saddle River, New Jersey, 1996).
- Brumberg, J.C., Pinto, D.J. & Simons, D.J. Spatial gradients and inhibitory summation in the rat whisker barrel system. *J. Neurophysiol.* **76**, 130–140 (1996).
- Brecht, M., Roth, A. & Sakmann, B. Dynamic receptive fields of reconstructed pyramidal cells in layers 3 and 2 of rat somatosensory barrel cortex. *J. Physiol. (Lond.)* **553**, 243–265 (2003).
- Armstrong-James, M. & Fox, K. Spatiotemporal convergence and divergence in the rat S1 “barrel” cortex. *J. Comp. Neurol.* **263**, 265–281 (1987).
- Swadlow, H.A. & Gusev, A.G. Receptive-field construction in cortical inhibitory interneurons. *Nat. Neurosci.* **5**, 403–404 (2002).
- Andermann, M.L., Ritt, J., Neimark, M.A. & Moore, C.I. Neural correlates of vibrissa resonance; band-pass and somatotopic representation of high-frequency stimuli. *Neuron* **42**, 451–463 (2004).

34. Chklovskii, D.B. Synaptic connectivity and neuronal morphology: two sides of the same coin. *Neuron* **43**, 609–617 (2004).
35. Laughlin, S.B. & Sejnowski, T.J. Communication in neuronal networks. *Science* **301**, 1870–1874 (2003).
36. Benison, A.M., Ard, T.D., Crosby, A.M. & Barth, D.S. Temporal patterns of field potentials in vibrissa/barrel cortex reveal stimulus orientation and shape. *J. Neurophysiol.* published online January 4, 2006 (doi:10.1152/jn.01034.2005).
37. Lichtenstein, S.H., Carvell, G.E. & Simons, D.J. Responses of rat trigeminal ganglion neurons to movements of vibrissae in different directions. *Somatosens. Mot. Res.* **7**, 47–65 (1990).
38. Lee, S.H. & Simons, D.J. Angular tuning and velocity sensitivity in different neuron classes within layer 4 of rat barrel cortex. *J. Neurophysiol.* **91**, 223–229 (2004).
39. Neimark, M.A., Andermann, M.L., Hopfield, J.J. & Moore, C.I. Vibrissa resonance as a transduction mechanism for tactile encoding. *J. Neurosci.* **23**, 6499–6509 (2003).
40. Moore, C.I. & Andermann, M.L. The vibrissa resonance hypothesis. *Somatosensory Plasticity* Ch. 2, 21–60 (CRC Press, Nashville, Tennessee).
41. Hartmann, M.J., Johnson, N.J., Towal, R.B. & Assad, C. Mechanical characteristics of rat vibrissae: resonant frequencies and damping in isolated whiskers and in the awake behaving animal. *J. Neurosci.* **23**, 6510–6519 (2003).
42. Brecht, M., Preilowski, B. & Merzenich, M.M. Functional architecture of the mystacial vibrissae. *Behav. Brain Res.* **84**, 81–97 (1997).
43. Land, P.W. & Erickson, S.L. Subbarrel domains in rat somatosensory (S1) cortex. *J. Comp. Neurol.* **490**, 414–426 (2005).
44. Timofeeva, E., Merette, C., Emond, C., Lavalley, P. & Deschenes, M. A map of angular tuning preference in thalamic barreloids. *J. Neurosci.* **23**, 10717–10723 (2003).
45. Wilent, W.B. & Contreras, D. Stimulus-dependent changes in spike threshold enhance feature selectivity in rat barrel cortex neurons. *J. Neurosci.* **25**, 2983–2991 (2005).
46. Huang, W., Armstrong-James, M., Rema, V., Diamond, M.E. & Ebner, F.F. Contribution of supragranular layers to sensory processing and plasticity in adult rat barrel cortex. *J. Neurophysiol.* **80**, 3261–3271 (1998).
47. Diamond, M.E., Huang, W. & Ebner, F.F. Laminar comparison of somatosensory cortical plasticity. *Science* **265**, 1885–1888 (1994).
48. Polley, D.B., Kvasnak, E. & Frostig, R.D. Naturalistic experience transforms sensory maps in the adult cortex of caged animals. *Nature* **429**, 67–71 (2004).
49. Stern, E.A., Maravall, M. & Svoboda, K. Rapid development and plasticity of layer 2/3 maps in rat barrel cortex *in vivo*. *Neuron* **31**, 305–315 (2001).
50. Bender, K.J., Rangel, J. & Feldman, D.E. Development of columnar topography in the excitatory layer 4 to layer 2/3 projection in rat barrel cortex. *J. Neurosci.* **23**, 8759–8770 (2003).